Observation of EHO in NSTX and theoretical study of its active control using HHFW antenna



2014 Nucl. Fusion 54 043013

(http://iopscience.iop.org/0029-5515/54/4/043013)

IOP Publishing | International Atomic Energy Agency Nuclear Fusion
Nucl. Fusion **54** (2014) 043013 (6pp) doi:10.1088/0029-5515/54/4/043013

# Observation of EHO in NSTX and theoretical study of its active control using HHFW antenna

**J.-K. Park[1], R.J. Goldston[1], N.A. Crocker[2], E.D. Fredrickson[1], M.G. Bell[1], R. Maingi[3], K. Tritz[4], M.A. Jaworski[1], S. Kubota[2], F. Kelly[a,1], S.P. Gerhardt[1], S.M. Kaye[1], J.E. Menard[1] and M. Ono[1]**

[1] Princeton Plasma Physics Laboratory, Princeton, NJ 08543, USA
[2] Institute of Plasma and Fusion Research, University of California, Los Angeles, CA 90095, USA
[3] Oak Ridge National Laboratory, Oak Ridge, TN 37831, USA
[4] Department of Physics and Astronomy, Johns-Hopkins University, Baltimore, MD 21210, USA

E-mail: jpark@pppl.gov

Received 9 January 2013, revised 3 January 2014
Accepted for publication 30 January 2014
Published 18 March 2014

**Abstract**

Two important topics for tokamak edge-localized modes (ELM) control, based on non-axisymmetric (3D) magnetic perturbations, are studied in NSTX and combined envisioning ELM control in the future NSTX-U operation: experimental observations of the edge harmonic oscillation (EHO) in NSTX (with lower frequency than EHOs in DIII-D and elsewhere), and theoretical study of its external drive using the high-harmonic fast wave (HHFW) antenna as a 3D field coil. EHOs were observed particularly clearly in NSTX ELM-free operation with very low $n$ core modes. A number of diagnostics have confirmed $n = 4$–6 edge-localized and coherent oscillations in the 2–8 kHz frequency range. These oscillations seem to have a favoured operational window in rotational shear, similar to EHOs in DIII-D quiescent H modes. However, in NSTX, they are not observed to provide significant particle or impurity transport, possibly due to their weak amplitudes, of a few mm displacements, as measured by reflectometry. The external drive of these modes has been proposed in NSTX, by utilizing audio-frequency currents in the HHFW antenna straps. Analysis shows that the HHFW straps can be optimized to maximize $n = 4$–6 while minimizing $n = 1$–3. Also, ideal perturbed equilibrium code calculations show that the optimized configuration with only 1 kAt current can produce comparable or larger displacements than the observed internal modes. Thus it may be possible to use externally driven EHOs to relax the edge pressure gradient and control ELMs in NSTX-U and future devices. Fine and external control over the edge pressure gradient would be a very valuable tool for tokamak control.

Keywords: tokamak, ELM, EHO, HHFW, 3D field

(Some figures may appear in colour only in the online journal)

## 1. Introduction

Edge localized modes (ELMs) can generate unacceptable heat loads to plasma-facing components in a reactor scale tokamak or spherical torus, and therefore ELM control is a critical issue for ITER [1, 2] and future devices. One promising concept is the application of steady non-axisymmetric (3D) fields, called resonant magnetic perturbations (RMPs). A leading hypothesis for the ELM-controlling effect of RMPs is that sufficiently strong 3D fields break nested flux surfaces and produce stochastic field lines, and thus maintain the pedestal pressure below the ELM stability boundary via enhanced particle transport [3]. While this hypothesis is challenged by a number of observations about ELM modifications and different correlations with particle transport [4–8], it is nonetheless believed that it will be best to align 3D field patterns with the equilibrium magnetic field pitch, and to place relevant coils as close as possible to the plasma, in order to produce strong resonant effects in the edge while minimizing penetration of the perturbations into the core. This imposes severe requirements for RMP coils, which may not be able to be met in a realistic fusion reactor, and thus it is valuable to identify alternative means of ELM control, such as operation in the quiescent H (QH) mode [9].

QH modes have been observed in various devices starting with DIII-D [9, 10], and followed by ASDEX-U [11], JET [11] and JT-60U [12]. The operational window for QH modes has

[a] When the work was done. Currently unaffiliated.

 

been significantly expanded [13, 14], but the extrapolation of this regime to ITER remains uncertain. Of greatest interest for present purposes is the replacement of ELMs by edge harmonic oscillations (EHOs) in QH modes, and the consequent reduction in the density gradient near the plasma edge.

It has been hypothesized that EHOs are peeling–ballooning modes destabilized by the strong rotational shear, but non-linearly saturated before ELM crashes through the decreased rotational shear caused by the modes themselves [26]. Although the natural EHOs are internally arising 3D fields, which drive particle transport, their specific requirement for edge rotational shear may limit their operational window. As a result, external 3D field applications may still be required to provide an adequate operational window through external rotation control [14]. The 3D coil requirement for this purpose may be less severe than that for RMPs in general, since the toroidal rotation profile is easier to modify with 3D fields than particle transport, since neoclassical toroidal viscosity (NTV) [15–17] does not require cross-field transport.

The mechanism of particle transport by EHOs has not been well understood. Enhanced particle transport has been inferred, only qualitatively, e.g. by the rate of rise of density or by $D_\alpha$ signal changes. The study in this paper proposes active drive of EHOs using the high-harmonic fast wave (HHFW) antenna, which can help further clarify and quantify the role of EHOs on particle transport and ELM modification under the direct control. In concern with this observation it should be recognized that since the mechanism of particle transport enhancement has not been yet identified, externally driven EHOs of a given amplitude may drive more or less transport than naturally occurring ones. The coil requirement for external EHO drive, however, appears to be consistent with the capabilities of ion-cyclotron antennas that are projected to be reactor-compatible.

Recent ELM-free NSTX [18] operations have produced clear harmonic oscillations in the plasma edge, which, however, did not appear to enhance particle or impurity transport. When these were first observed in 2010 (by Goldston), it was proposed that the EHOs on NSTX might be too weak to drive transport and that these modes might be amplified by coupling of either modulated high-frequency power from the NSTX HHFW antenna or by audio-frequency drive using the same antenna structures. This study shows that audio-frequency currents driven through the HHFW antenna in NSTX [19] can indeed be favourable for the purpose. Although the motivation for this study in part relies on the assumption that particle transport is correlated positively with amplitudes of EHOs, the implementation of EHO drive will allow this hypothesis to be tested. This paper is organized as follows: experimental observations on EHOs will be described in section 2, and the theoretical study of its audio-frequency active control using the NSTX HHFW antenna will be discussed in section 3, with concluding remarks following in section 4.

## 2. Observation of EHO in NSTX

Plasma confinement in NSTX has been significantly improved with lithium wall coatings and the associated stabilization of various ELMs. The energy confinement time increases and edge electron thermal diffusivity decreases almost linearly

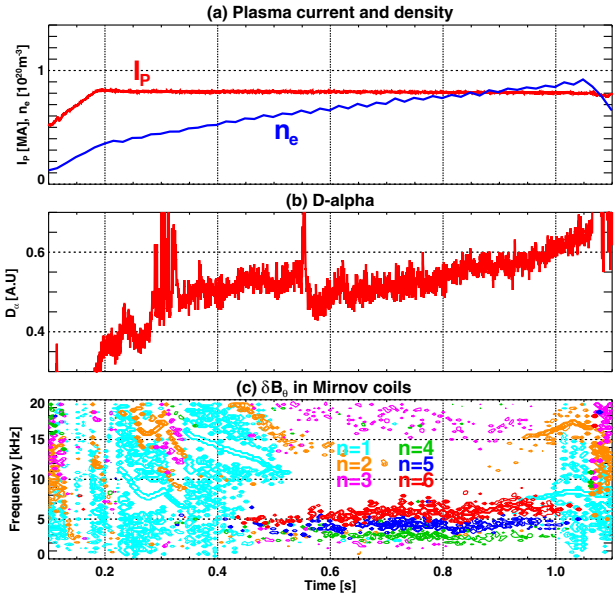


**Figure 1.** An example of the EHOs observed in NSTX (#138239). One can see the clearly separated $n = 4$–6 harmonic oscillations in the ELM-free state at $t = 0.5 \sim 1.0$ s, with 2–8 kHz frequency range, from ($c$) magnetic oscillations detected in Mirnov coils.

with pre-discharge lithium evaporation rate [20], and type-I ELMs can be almost eliminated when the lithium deposition is sufficiently strong [21]. If operational conditions are further adjusted to suppress other small ELMs, such as the type-II or even the type-V, a long ELM-free operation can be achieved in NSTX [22]. Clear EHOs were observed under such ELM-free conditions, reproducibly through a large number of discharges.

Figure 1 shows an example, with ~4 MW of neutral beam injection (NBI) power, $I_P \sim 800$ kA plasma current and $B_T \sim 4.5$ kG. One can see the absence of ELMs during a long period, $t = 0.5$–1 s, from panel ($b$), and clear oscillations with low frequency 2–8 kHz and intermediate toroidal periodicity $n = 4$–6 from the panel ($c$), the Mirnov signals. The Mirnov coil measurements are specially tuned to low frequency and low amplitudes in order to capture the relatively weak amplitudes of the intermediate $n$ modes compared with typical low $n$ mode activities. These long-lived oscillations in fact can be observed under other conditions transiently, as reported in the type-V ELM operating regime [23] with partially similar characteristics, but can be found mostly clearly and strongly under the particular operating conditions described here.

The oscillations were also found in other diagnostics, which all suggest the edge-localized and coherent nature of the oscillations. The ultrasoft x-ray (USXR) [24] in figure 2($a$) used 5 $\mu$m of beryllium foil for filtering the diode array channels, which is thinner than the conventional 10 $\mu$m or 100 $\mu$m filters, in order to detect low energy at the end of the pedestal region. One can see that this edge USXR also shows the oscillations in the similar frequency range 2–8 kHz. Although the oscillations appeared a bit later than the Mirnov signals due to the difficulty in resolving the weak amplitudes of the intermediate $n$ when the low $n$ modes are active, the three frequency bands correspond well to the $n = 4$–6 modes in the Mirnov signals after $t = 0.6$ s. The oscillations are even observable in the far scrape-off layer (SOL) region, as

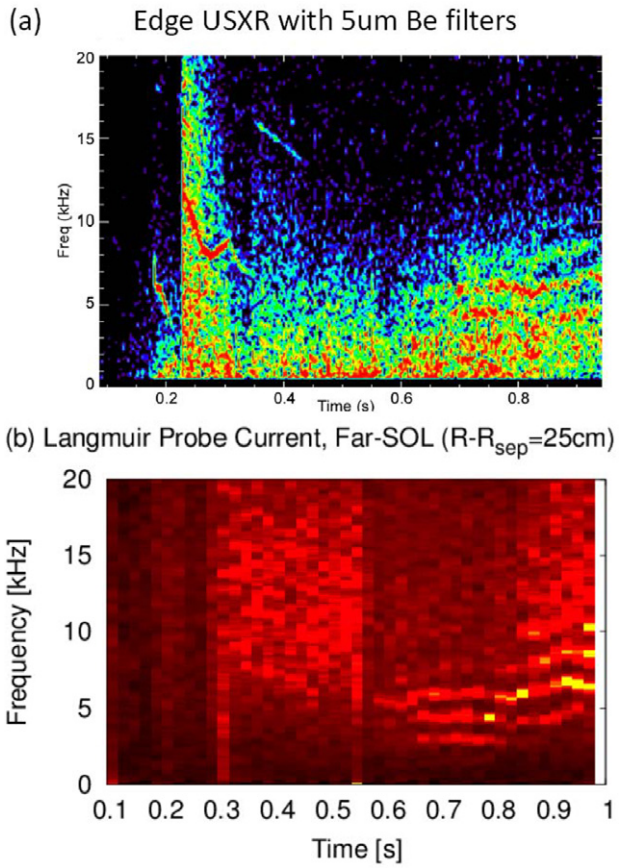


**Figure 2.** EHOs observed in the same discharge #138239 as shown in figure 1, by (*a*) the edge USXR, and (*b*) the Langmuir probes in the far SOL. One can see three bands corresponding to the $n = 4$–6 in the Mirnov signals after $t = 0.6$ s, in the similar frequency range 2–8 kHz.

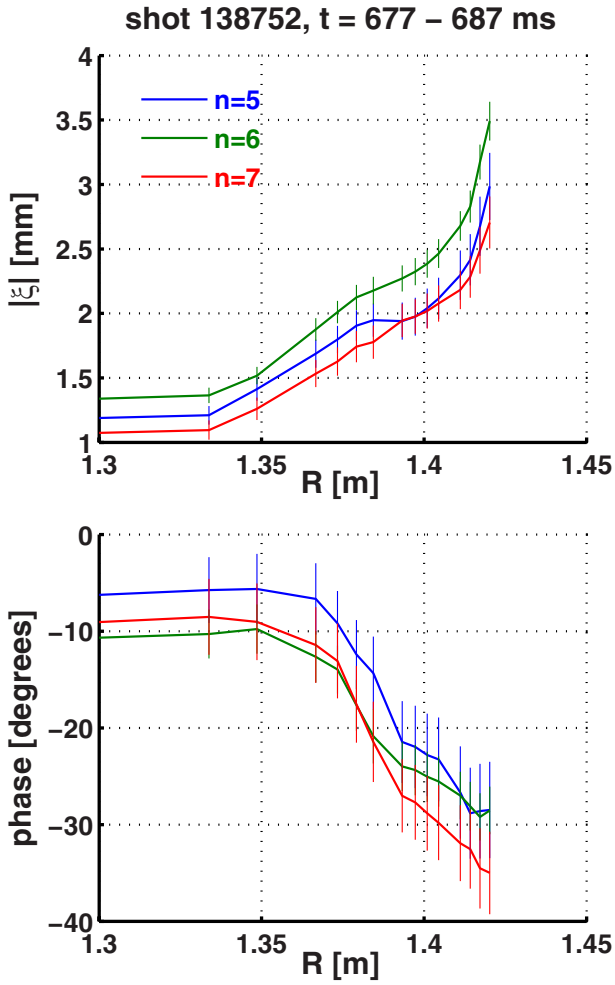


**Figure 3.** Plasma displacement profiles associated with the EHOs in NSTX, measured by reflectometer in the discharge #138752. The edge localized nature can be seen from (*a*) the amplitude. There are some radial variations in (*b*) the phase.

can be seen in figure 2(*b*), which shows the fluctuations in the ion saturation current measured by triple Langmuir probes (LPs) at the divertor floor located away from the separatrix by $R = 25$ cm [25].

These two measurements, the USXR and far SOL LPs, indicate the presence of the modes in the edge but not the edge-localized characteristics, although they indicate the coherent nature of the modes as the detected frequency range is all similar. However, one can evaluate the mode location by the mode frequency, if one assumes the mode rotation is equivalent or similar to the plasma rotation. Then from $f(n = 5) \sim 5$ kHz as shown by above examples, the plasma rotation can be estimated as ~1 kHz. This rotation frequency is even smaller than the carbon rotation at the last data point in the edge from charge-exchange recombination spectroscopy (CHERS), but the extrapolation indicates that the modes may be very close to the last close flux surfaces. It will be interesting to measure the poloidal structure of the modes in the future to see if $q \sim m/n$ holds as expected from resonant MHD modes such as EHOs [26].

The edge-localized nature of the oscillations becomes more evident by reflectometer measurements. Figure 3 shows the amplitude and temporal phase of the oscillating *effective displacement* of each mode measured using a 16-channel array of fixed frequency quadrature reflectometers [27]. Effective displacement, defined as half the millimetre-wave path length fluctuation, is approximately equal to displacement of the millimetre-wave cutoff location in regions of steep density gradient, as for the measurements shown here. For the circumstances of this measurement, effective displacement is approximately displacement of the plasma flux surfaces. The reflectometer array used frequencies in the range 30–75 GHz operating with O-mode polarization, corresponding to cutoffs at densities of $n_0 = 1.1$–$7.0 \times 10^{19}$ m$^{-3}$. For O-mode polarization, the displacement of the cutoff location is the displacement of the cutoff density contour which, in the absence of plasma compression, is caused by the displacement of the plasma flux surface. One can see in figure 3 that the displacement peaks strongly at $R > 1.35$ m, which corresponds to the pedestal gradient region inside the separatrix located at $R \sim 1.47$ m, The mode amplitudes are up to 3–4 mm. Also, the modes are coherent, although it is not shown here, as indicated by their simultaneous observation by the reflectometers and edge b-dot coils distributed around the torus. It is interesting that the reflectometry shows $n > 6$ modes which are beyond the observed range on the Mirnov signal. Still the $n = 6$ mode is the largest, but this observation

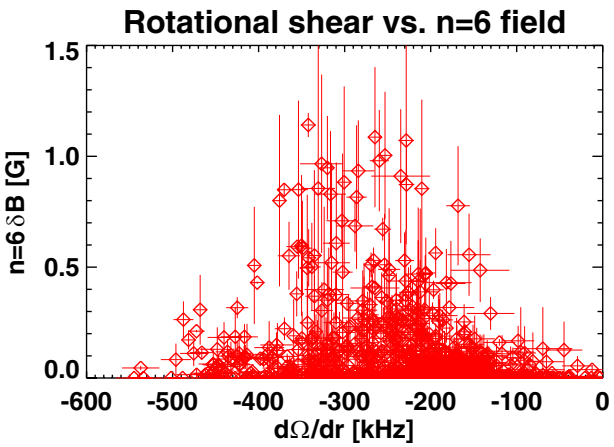


**Figure 4.** Statistical analysis indicating the $n = 6$ of the EHOs in NSTX may have an optimal range of the rotational shear at the end of the pedestal ($R \gtrsim 1.45$ m).

indicates that the NSTX EHOs maybe included in the coherent toroidal harmonic modes over a range wider than $n = 4$–6. In some discharges, modes from $n = 2$ to 6 have been observed on the Mirnov signals. In general the harmonics are fairly evenly spaced in frequency, typically with $\Delta f/\Delta n \sim 1.5$–2.5 kHz, which is significantly lower than the higher-field conventional aspect-ratio tokamaks. In general as well, the extrapolation of $f$ to $n = 0$ does not give $f = 0$. For example in the discharge shown here, the $n = 4$ mode is at about 3 kHz, while the $n = 6$ mode is at about 6 kHz, so the extrapolation to $n = 0$ gives approximately $-3$ kHz.

The coherent EHOs found in NSTX, while not necessarily identical to the EHOs in DIII-D, may have similar stability characteristics. The EHOs on DIII-D are understood to be intermediate $n$ peeling modes destabilized by strong rotational shear and non-linearly saturated by self-regulation of the rotation shear [26]. The EHOs in NSTX are also mostly at intermediate $n$'s, indicating that they may also be associated with peeling modes. Moreover, stability analysis using the DCON code [28] indicates that the studied discharges are close to marginal stability for $n > 3$ and thus $n > 3$ modes would be easily triggered if any non-ideal MHD destabilizing mechanism is present. In NSTX, the EHOs become apparent under particular operating conditions, such as the beam power ~4 MW as mentioned earlier in this paper, and these operational conditions may be linked to particular kinetic parameters such as the rotational shear. Indeed, the statistical analysis of the Mirnov sensor signals for ~30 discharges shows the possible linkage between the mode amplitudes and the rotational shear, as can be seen in figure 4. That is, although the correlation is not strong, an optimal range of the rotational shear seems to exist for the NSTX EHOs. This correlation with the rotational shear is one of the important characteristics for low-$n$ peeling stability and EHOs, as found in ELITE code applications to the DIII-D QH modes [26].

These oscillations, however, did not provide significant particle transport or impurity control in NSTX, unlike the EHOs in the DIII-D QH modes. For instance, the particle density is still rising while these EHOs are active, as can be seen in figure 1($b$). Also $D_\alpha$ signal in figure 1($c$) does not apparently show an increase in the baseline nor an indication of any particle transport enhancement. This functional difference of the modes between two devices was also experienced in the comparison tests of enhanced D-alpha (EDA) H-modes between the C-Mod and the DIII-D tokamaks. The quasicoherent mode (QCM), which was identified as the source of the enhanced particle transport in C-Mod, was also found similarly in DIII-D but its drive of particle transport was not enough to maintain a steady-state H-mode [29]. The EHOs are distinguished from the QCMs by their multiple-harmonics and lower frequencies of the modes as described here, but it is interesting to see from both that the actual utility for particle control can largely differ across devices.

A reasonable assumption to explain the difference is that the modes in one device may be not strong enough to modify particle transport, unlike the other. In fact, the mode amplitudes measured by the Mirnov coils in NSTX, as shown in figure 4, are quite a bit smaller than the EHOs in DIII-D, where $\delta B \sim 10$ G were often reported by the Mirnov coils [10]. Assuming the Mirnov signal amplitude approximately equal to the mode amplitude at the outboard midplane, where the wavelength of the edge mode is large compared with the distance to the outboard Mirnov coils in both machines, the level of perturbations by the EHOs in NSTX is $\delta B/B_0 \sim 2 \times 10^{-4}$, but $\delta B/B_0 \sim 5 \times 10^{-4}$ in DIII-D. This implies that the EHOs in NSTX can become similar in normalized amplitudes to DIII-D if they are amplified by several factors and then may perhaps enhance particle transport, albeit with the caveats noted above. This hypothesis can be tested with appropriate amplifying tools such as the HHFW antenna, as will be described in the next section.

## 3. Study of edge-harmonic mode control using HHFW antenna

It has been proposed that the amplification of the EHOs in NSTX may be possible, if it is possible to couple to these modes by audio-frequency currents in the antenna straps. The HHFW antenna locations are localized within a 90° toroidal section and so they can effectively drive intermediate $n$ modes in the edge. Figure 5($a$) shows the illustration of the HHFW antenna straps. The straps are composed of 12 toroidal arrays, but each array can be separated through the ground (White) in the middle and so there are 24 straps in total. One can model these HHFW antenna straps including each filament as shown in figure 5($b$) and treat them as a set of 3D coils. Compared with the existing resistive wall mode and error field correction (RWMEF) coils, one can see the small apertures, the proximity to the plasma, and the localized nature, suggesting the effectiveness for higher $n$ magnetic perturbations. The straps will be supplied by a limited number of power supplies, and thus the connection and configuration needs to be optimized.

The optimization should be assessed based on its effectiveness in driving higher $n > 3$ modes while minimizing the low $n = 1$–3 modes. Our quantification for the optimization is based on the coupling between the dominant mode and the applied field by the HHFW straps, for each $n$. The dominant external field is defined as the field maximizing the resonant responses and can be identified using the ideal perturbed equilibrium code (IPEC) [30, 31]. Then the coupling

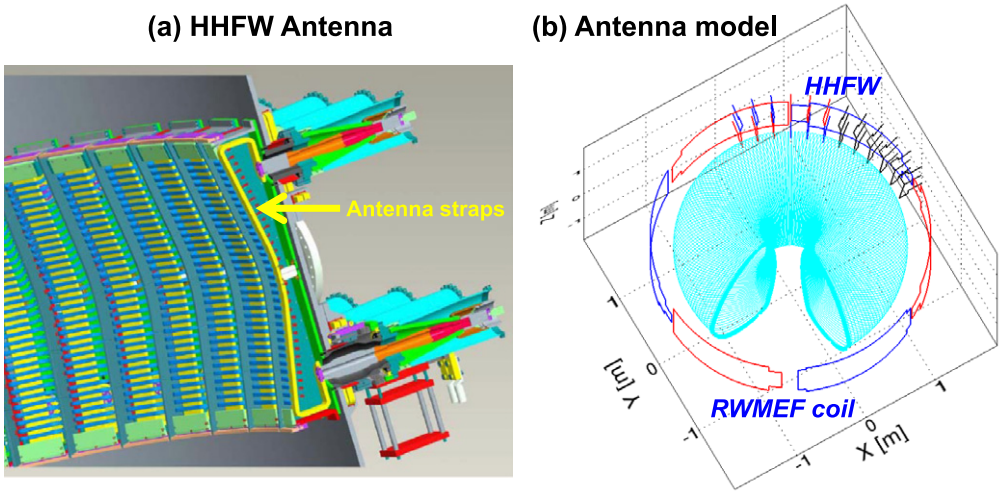


**Figure 5.** The design of the NSTX HHFW antenna in (*a*), and the filament model of the antenna straps in (*b*), compared with the existing resistive wall mode and error field correction (RWMEF) coils. The colour codes in (*b*) show the finally optimized configuration for $n = 4$–6, as described in the paper.

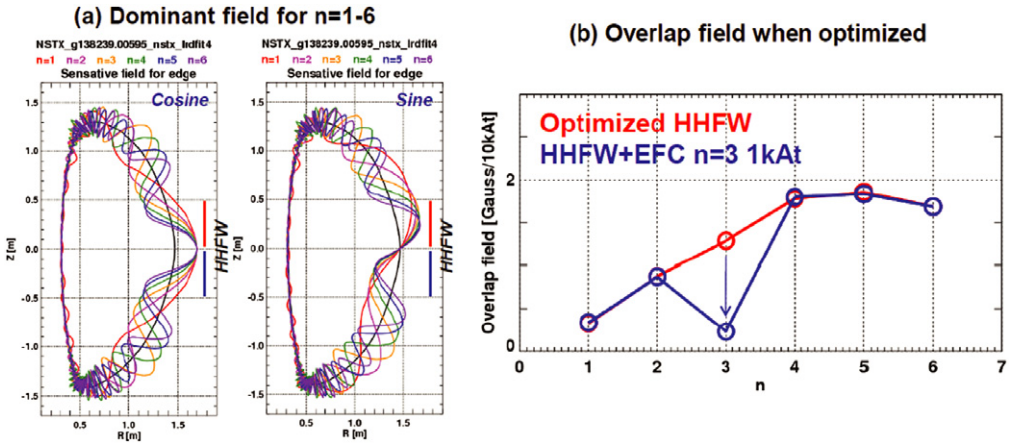


**Figure 6.** IPEC analysis for the (*a*) dominant $n = 1$–6 external field measured on the plasma boundary, and the (*b*) overlap with the dominant field when the configuration is optimized for high $n = 4$–6. In principle, the RWMEF coil can be used to reduce $n = 1$–3 further, as illustrated in (*b*).

with the applied field can be calculated by the overlap integral between the two different field distributions on the plasma boundary [32]. Calculations have been performed for each configuration giving the overlap field for each $n$, and the effectiveness of the configuration can be assessed by the overlap fields for $n = 4$–6 while minimizing the overlap fields for $n = 1$–3.

Figure 6(*a*) shows the structure of the dominant external field for each $n$ for the cosine part $C(\theta)$ and the sine part $S(\theta)$ which can be combined to represent the 3D field as $\delta B_n = C(\theta)\cos(n\phi) + S(\theta)\sin(n\phi)$. One can see that the wavelength, especially of the sine part, becomes comparable to the vertical length of a single strap for higher $n$, indicating significant capability of HHFW straps for driving the higher $n$ modes.

The next step is to vary the strap configuration and calculate the applied field and the overlap with the dominant field. Among a number of combinations, additional considerations are (1) assuming just one power supply, which means all the straps should have the same amplitude of currents, and (2) reducing the number of active straps as much as possible to mitigate the complexity of the system. After the investigation of many different combinations, the optimized configuration was found to be to use 12 straps with polarity switching by three-strap blocks, as colour coded in figure 5(*b*).

The current amplitude will be limited, so it is important to know how much current is actually required to drive and amplify the modes by a factor of a few with the optimized configuration. IPEC can provide magnetic field and displacement perturbed by the HHFW antenna straps, and particularly plasma displacement calculations can be compared with the reflectometry data. As discussed earlier, an important goal of the study is to amplify the modes actively by the HHFW antenna, and to see if the mode amplitude increased in this manner can drive particle transport and actually modify pedestal and edge stability.

Figure 7 shows IPEC prediction for $n = 5, 6$ modes at the midplane with 1 kAt amplitudes for each strap, in the pedestal up to the separatrix at $R \sim 1.47$ m, compared with the reflectometer measurement. Note that $n = 5$ shows much stronger plasma amplification than $n = 6$ in this particular

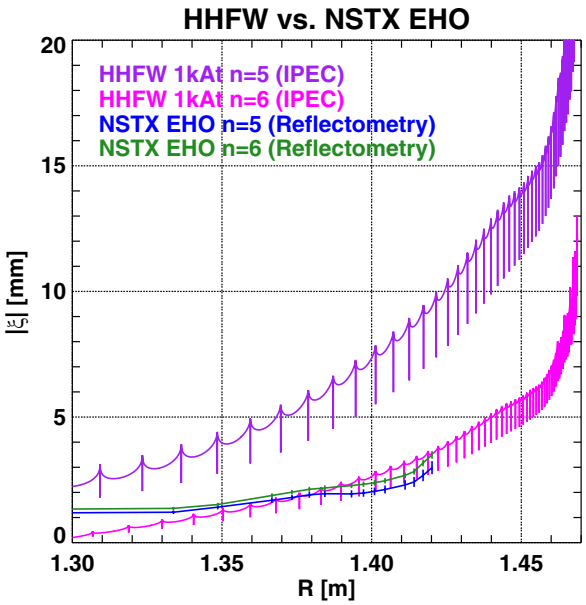


**Figure 7.** The externally driven displacements by the optimized HHFW antenna configuration, predicted by IPEC, and the internally driven displacements by the EHOs in NSTX, measured by reflectometry. The comparison is shown for the pedestal inside the separatrix at $R \sim 1.47$ m.

example, but this should not be generalized as the high $n$ responses can be sensitive to the profile reconstruction in the edge. One may also be curious about the sharp peaks in the IPEC results. The peaks represent the discontinuity across the rational surfaces due to the ideal constraints. Each rational surface requires a very high and adaptive spatial grid. The total radial grid number is almost up to $10^4$ with the poloidal grid up to $10^3$ since there are many rational surfaces for high $n$ in NSTX due to high $q_{95}$. For example, there are almost 100 rational surfaces for $n = 6$. Therefore, the computational cost is quite demanding even though IPEC is a linear and fast code, which limited the number of cases that could be tested. Nevertheless, those tests showed that the $n = 4$–6 can vary from the few mm to ~10 mm depending on the discharge or the reconstruction method.

In general, one can conclude that IPEC predicts comparable or larger by a factor of a few displacements for the $n = 4$–6 when the optimized configuration is selected, only with 1 kAt, which is not very demanding for an audio-frequency power supply. Our expectation is that the external drive tuned to the same $n$ and frequency range as the internally arising mode may directly amplify the internal modes and possibly lead to enhanced particle transport and ELM stability modification.

## 4. Concluding remarks

The observation of the edge harmonic oscillation in NSTX, and the theoretical study of its active drive using HHFW antenna as a 3D coil have been presented and discussed. The possibility of implementing a drive system will be examined in NSTX-U first, and successful demonstration of density and impurity control would provide a pathway to audio-frequency current drive of peeling–ballooning modes for edge particle and ELM control in future devices, including perhaps ITER. In principle, this can be a powerful and unique tool for ELM control in tokamaks, compared with utilizing externally driven quasi-steady 3D fields for ELM suppression and/or rotation control and/or relying on internally driven 3D fields.

## Acknowledgment

This work was supported by DOE Contract No DE-AC02-09CH11466.

## References

[1] Shimada M. 2007 *Nucl. Fusion* **47** S1
[2] Hawryluk R. *et al* 2009 *Nucl. Fusion* **49** 065012
[3] Evans T.E. *et al* 2004 *Phys. Rev. Lett.* **92** 235003
[4] Evans T. *et al* 2008 *Nucl. Fusion* **48** 024002
[5] Fenstermacher M.E. *et al* and the DIII-D Team 2008 *Phys. Plasmas* **15** 056122
[6] Canik J.M. *et al* and the NSTX Research Team 2009 *Phys. Rev. Lett.* **104** 045001
[7] Suttrop W. *et al* and the ASDEX Upgrade Team 2011 *Phys. Rev. Lett.* **106** 225004
[8] Jeon Y.M. and Park J.-K. 2012 *Phys. Rev. Lett.* **109** 035004
[9] Burrell K.H. *et al* 2001 *Phys. Plasmas* **8** 2153
[10] Burrell K.H. *et al* 2005 *Phys. Plasmas* **12** 056012
[11] Suttrop W. *et al*, the ASDEX Upgrade Team and Contributors to the JET-EFDA Workprogramme 2005 *Nucl. Fusion* **45** 721
[12] Oyama N. *et al* and the JT-60 Team 2005 *Nucl. Fusion* **45** 871
[13] Burrell K.H., Osborne T.H., Snyder P.B., West W.P., Fenstermacher M.E., Groebner R.J., Gohil P., Leonard A. and Solomon W.M. 2009 *Phys. Rev. Lett.* **102** 155003
[14] Burrell K.H., Garofalo A.M., Solomon W.M., Fenstermacher M.E., Osborne T.H., Park J.-K., Schaffer M.J. and Snyder P.B. 2012 *Phys. Plasmas* **19** 056117
[15] Shaing K.C. 1983 *Phys. Fluids* **26** 3315
[16] Zhu W. *et al* 2006 *Phys. Rev. Lett.* **96** 225002
[17] Park J.-K., Boozer A.H. and Menard J.E. 2009 *Phys. Rev. Lett.* **102** 065002
[18] Ono M. *et al* and the NSTX Team 2000 *Nucl. Fusion* **40** 557
[19] Taylor G. *et al* 2010 *Phys. Plasmas* **17** 056114
[20] Maingi R. *et al* 2011 *Phys. Rev. Lett.* **107** 145004
[21] Maingi R. *et al* and the NSTX Research Team 2009 *Phys. Rev. Lett.* **103** 075001
[22] Maingi R., Hubbard A., Meyer H., Hughes J., Kirk A., Maqueda R., Terry J., the Alcator C-Mod MAST and NSTX Teams 2011 *Nucl. Fusion* **51** 063036
[23] Sontag A. *et al* 2011 *Nucl. Fusion* **51** 103022
[24] Stutman D., Finkenthal M., Moos H.W., Fournier K.B., Kaita R., Johnson D. and Roquemore L. 2003 *Rev. Sci. Instrum.* **74** 1982
[25] Jaworski M.A., Kallman J., Kaita R., Kugel H., LeBlanc B., Marsala R. and Ruzic D.N. 2010 *Rev. Sci. Instrum.* **81** 10E130
[26] Snyder P. *et al* 2007 *Nucl. Fusion* **47** 961
[27] Crocker N.A. *et al* 2011 *Plasma Phys. Control. Fusion* **53** 105001
[28] Glasser A.H. and Chance M.S. 1997 *Bull. Am. Phys. Soc.* **42** 1848
[29] Mossessian D.A., Groebner R.J., Moyer R.A., Osborne T.H., Hughes J.W., Greenwald M., Hubbard A. and Rhodes T.L. 2003 *Phys. Plasmas* **10** 689
[30] Park J.-K., Boozer A.H. and Glasser A.H. 2007 *Phys. Plasmas* **14** 052110
[31] Park J.-K., Boozer A.H., Menard J.E. and Schaffer M.J. 2008 *Nucl. Fusion* **48** 045006
[32] Park J.-K., Schaffer M.J., La Haye R.J., Scoville T.J. and Menard J.E. 2012 *Nucl. Fusion* **52** 089501